ADVANCED PRESSURE BOUNDARY MATERIALS

Michael Santella
Oak Ridge National Laboratory, 1 Bethel Valley Road, Oak Ridge, Tennessee, 37831-6096
Email: santellaml@ornl.gov; Telephone: 865-574-4805

John Shingledecker
Oak Ridge National Laboratory, 1 Bethel Valley Road, Oak Ridge, Tennessee, 37831-6155
Email: shingledecjp@ornl.gov; Telephone: 865-574-5108

ABSTRACT

Synchrotron diffraction experiments were conducted to examine the real-time transformation behaviour of an experimental 9Cr-3W-3Co-NbV steel with high B and low N (N130B), and the commercial P92 steel under simulated weld heat-affected zone thermal cycles. When heated to peak temperatures near 1100°C, both steels rapidly transformed from ferrite to 100% austenite. During cooling, both transformed to martensite near 400°C. Both steels also retained untransformed austenite: 1.7% in N130B and 5.8% in P92. When N130B was heated to about 60°C above its A_3 of 847°C about 56% of the original ferrite never transformed to austenite. During cooling an additional 21% of ferrite and 23% of martensite formed. It retained no austenite. When P92 was heated to just above its A_3 of 889°C about 15% of its original ferrite never transformed to austenite. During cooling an additional 22% of ferrite and 60% of martensite formed. This steel retained about 2.3% of austenite. Metallographic examinations indicated that the $M_{23}C_6$ in N130B was much more stable than that in P92 for heating to the lower peak temperatures. Analysis using equilibrium thermodynamics suggested that the more stable $M_{23}C_6$ in N130B could raise its apparent A_3 by sequestering C. This could cause the ferrite-austenite transformation to appear sluggish. Thermodynamic analysis also indicated that the $M_{23}C_6$ in N130B contained about 3.9 at% B compared to about 0.08 at% B in that of P92. In contrast, the Mo and W content of the $M_{23}C_6$ was predicted to be higher in P92.

INTRODUCTION

Much of the high strength of the 9 wt% Cr steels being developed for power generation applications is related to their low temperature (< 1000°C) phase transformation behaviour. The Cr, added primarily for oxidation/corrosion resistance, has the important side effect of increasing hardenability, i.e., the ease with which martensite can form in the alloys [1]. The result of alloying and processing is that martensitic steels are produced after normalizing treatments consisting of a high temperature solution treatment followed by air cooling. The as-normalized martensitic structure is composed of fine laths, typically < 1 μm wide x many microns long. The laths contain dense dislocation tangles generated by the plastic accommodation of strain during the austenite-to-martensite transformation [1]. Finally, the martensitic microstructures are tempered to develop the desired mechanical properties.

Tempering tends to promote both recovery of the dislocation substructure and precipitation of particles based on $M_{23}C_6$ and M(C,N) [2,3,4,5]. Ideally, tempering causes the dislocation substructure to recover into a subgrain structure. The $M_{23}C_6$ particles tend to precipitate on prior austenite grain boundaries and subgrain boundaries pinning them [3,4]. The M(C,N) particles also precipitate on boundaries, but they may be uniformly distributed throughout the matrix as well [4]. The M(C,N) particles pin dislocations and impede their motion. The remarkable strength properties of these martensitic steels derive finally from the combination of dislocation hardening, particle hardening, and solid solution hardening [4].

The fact that martensitic steels respond to tempering with microstructure-property changes has disadvantages as well. One source of concern originates with the localized heating that accompanies welding. Welding produces gradients in the unmelted base metal where temperatures decrease from the melting point (near 1500°C) to the ambient welding temperature (up to 200-300°C) over distances of a few millimetres. This heat-affected zone (HAZ) experiences highly dynamic microstructure changes, one consequence of which is that a small region of relatively weak material typically forms between the weld deposit and the unaffected base metal [6]. The weakened HAZ regions tend to be failure initiation sites whenever welds are loaded transversely at low stresses (< 100 MPa) and high temperatures (< 650°C). This is the type of behaviour referred to as Type IV failure [7,8].

There are considerable economic and environmental benefits in understanding, controlling, and eliminating the causes of Type IV failure in martensitic steels because it limits their potential advantages in power generation systems [9]. Recent studies indicate that B additions coupled with control of N levels can suppress the Type IV failure mechanism in welded 9Cr steels [10,11,12]. Several mechanisms were suggested as possible explanations for this behaviour, but the reasons for it are still unclear. With this in mind the present work was done to investigate the austenite-ferrite transformation behaviour in more detail. Synchrotron diffraction experiments were used determine ferrite and austenite phase fractions of a commercial 9Cr steel (P92) and a Type-IV-resistant 9Cr-3W-3Co-NbV steel with high B and low N (N130B) during simulated weld thermal cycles.

EXPERIMENTAL DETAILS

The chemical compositions of the two 9Cr steels that were used are given in Table 1. The alloys were supplied in normalized-and-tempered (N+T) condition: 1 h @ 1080°C + 1 h @ 800°C for the boron-steel N130B and 2 h @ 1070°C + 2 h @ 780°C for the P92 steel. Specimens with dimensions of 1 mm x 4.8 mm x 112 mm were used where the diffracting surfaces were metallographically polished.

Table 1 Chemical compositions

	Element (wt%)										
ID	C	Si	Mn	Cr	W	Mo	Co	Nb	V	N	B
N130B	0.077	0.30	0.49	8.97	2.87	---	2.91	0.046	0.18	0.0015	0.013
P92	0.09	0.16	0.47	8.72	1.87	0.45	---	0.06	0.21	0.050	0.002

Full details about the synchrotron experiments including data analysis procedures are available from previous reports and from Elmer et al [13].

To select peak temperatures for the diffraction experiments, the HAZ temperatures were calculated using a 3D Rosenthal analysis and then compared to the A_1 and A_3 temperatures estimated from equilibrium thermodynamics calculations using the Thermo-Calc software and a Thermotech database [14]. The calculated A_1 and A_3 temperatures are given in Table 2.

Because of the limitation of data collection at 3 s intervals, the heating rates were adjusted to reach the peak temperatures in 9 s so that a few diffraction patterns were captured during heating. The 3 s dwell was added to capture at least one diffraction pattern at the peak temperatures. Ultimately, there were some discrepancies between the programmed and actual peak temperatures as shown in Table 3.

Microstructures of the heat treated specimens were examined optically and by scanning electron microscopy.

Table 2. A_1 and A_3 transformation temperatures estimated from equilibrium thermodynamics calculations

	Temperature (°C)	
Steel	A_1	A_3
N130B	817	847
P92	824	889

Table 3. Comparison of programmed and actual peak temperatures

	Peak temperature (°C)	
Experiment	Programmed	Actual
N130B-1	843	911
N130B-4	1100	1122
P92-1	843	896
P92-4	1100	1088

RESULTS

Specimens of both steels that were heated to the highest simulated HAZ peak temperatures rapidly transformed from ferrite to austenite and were completely austenitized. As expected, on cooling, austenite was retained well below the respective A_1s until the M_Ss were reached in the vicinity of 400°C. Diffraction was continued until the specimens were below 40°C. At that point both steels retained small amounts of austenite, about 1.7% for N130B and about 5.8% for P92. Overall, the transformation behaviour agreed with conventional expectations about what will happen in weld HAZs.

The results for specimens that were heated to the lowest peak temperatures are shown in Figure 1. As indicated, the peak temperature for the N130B was 911°C, a temperature about 60°C higher than the calculated A_3. The peak temperature for the P92 specimen was 896°C which is just at its calculated A_3. In both steels, relative to welding, these temperatures would be considered representative of the fine-grained HAZ region. For these thermal history conditions there is a significant difference in the transformation behaviour of the two steels, and overall it was more complicated than expected.

For the N130B, Figure 1 indicates that the maximum amount of austenite formed was 44%. This means that 56% of the original ferrite (tempered martensite) never transformed to austenite. During cooling, before the M_S was reached the amount of ferrite increased another 21%. The ferrite grows because it is the stable phase below A_1, and because there is no nucleation barrier to its formation. When the M_S was finally reached the remaining austenite transformed to martensite. This transformation sequence resulted in a microstructure composed of 56% of the original ferrite, 21% of newly grown ferrite, and 23% of martensite. No retained austenite was detected in this specimen.

In contrast, Figure 1 shows that the P92 transformed to about 85% austenite for the indicated thermal cycle. About 15% of the original ferrite never transformed. During cooling between the peak temperature and M_S the amount of ferrite further increased by about 22%. Eventually, the austenite transformed to about 60.4% martensite. About 2.3% of austenite was retained in the microstructure.

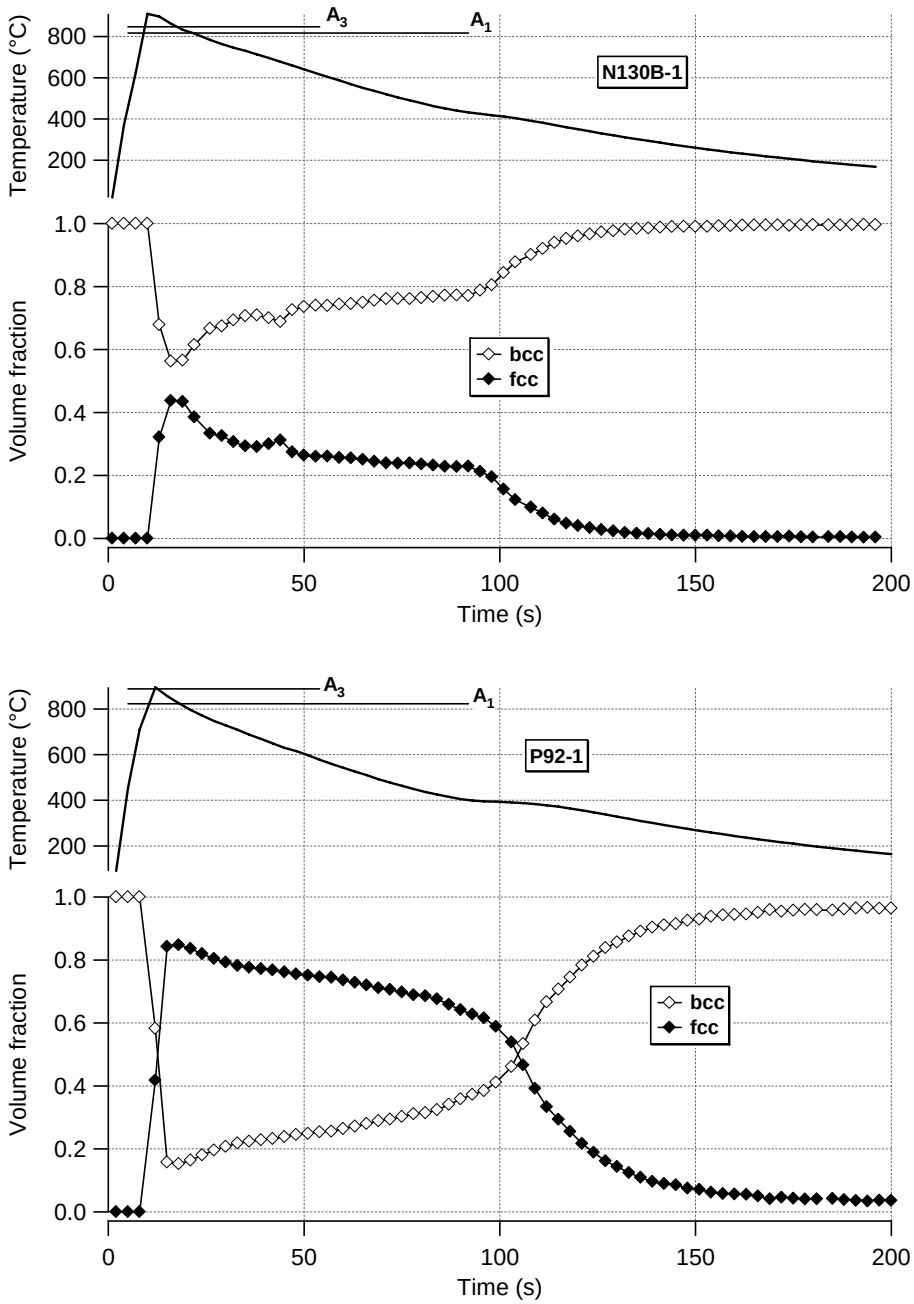

Figure 1 Plots of temperature and corresponding bcc and fcc phase fractions with time for (top) N130B with peak temperature of 911°C, and (bottom) P92 with peak temperature of 896°C

The original microstructures of both alloys were characteristic of the N+T condition in these types of steels. Subgrain boundaries and prior austenite grain boundaries were clearly delineated by carbide precipitation. Consistent with other observations [10,11,12], the prior austenite grain size of the N130B steel was somewhat larger than that of the P92.

The effects on the microstructures of N130B and P92 of heating through the thermal histories shown in Figure 1 are illustrated by the optical micrographs of Figure 2. Many carbide particles are still visible

along subgrain boundaries and prior austenite grain boundaries in N130B. The original tempered martensite structure appears largely preserved and many of the original prior austenite grain boundaries are clearly visible. There are also regions, like the one outlined in Figure 2, near some prior austenite grain boundaries where carbide dissolution is apparent, and where it appears that the original tempered martensite structure was replaced by new martensite. In the P92, prior austenite grain boundaries are still faintly visible and these appear decorated by carbides. However, the original subgrain structure is no longer visible, and there is no clear indication that carbides are present except on the austenite grain boundaries. The general structure appears martensitic, but small grains that appear to be ferrite are also present.

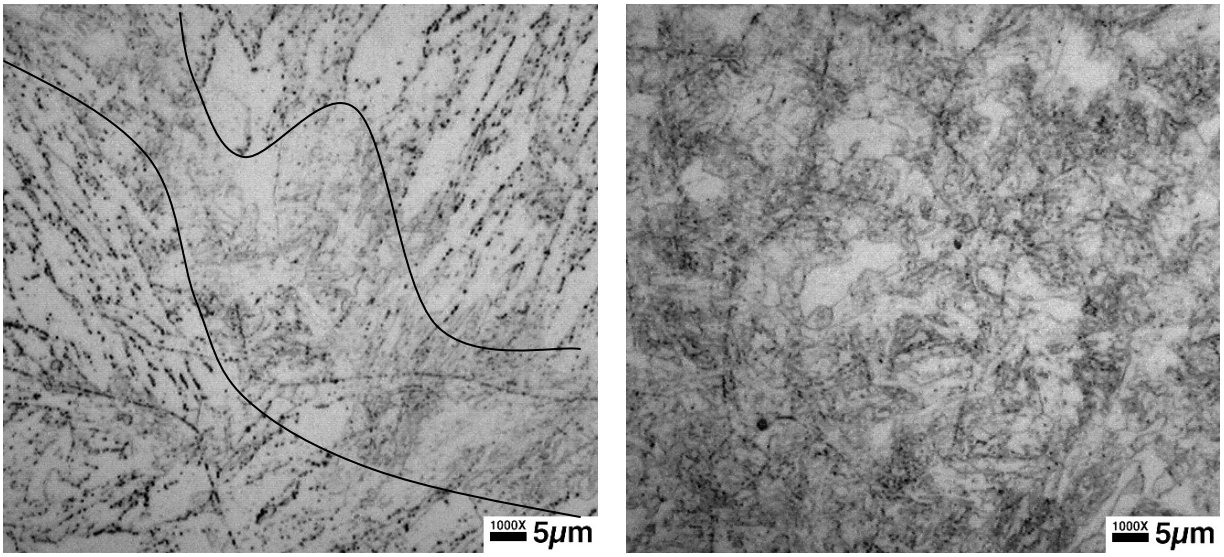

Figure 2 Optical micrographs showing the microstructures of (top) N130B and (bottom) P92 after heating through the respective thermal cycles shown in Figure 1

More details of these last two structures are shown in the secondary electron SEM images presented in Figure 3. Carbide particles are clearly evident in N130B. They are widely distributed through the microstructure except for the grain extending from the lower left corner of the micrograph. This feature appears to be a ferrite grain. Carbide particles are also evident in the P92 specimen, especially outlining the prior austenite grain boundaries. Otherwise, there are few carbides distributed throughout the microstructure. Grains showing little internal structure are visible and these presumably are ferrite. The bulk of the microstructure appears composed of martensite containing few visible carbides.

Vickers indentation with a 200 g load was used to measure the hardness of the specimens from Figure 2. The measured values were 2.57 GPa for N130B, and 4.02 GPa for P92. These hardnesses are consistent with interpretation of the diffraction data and metallography.

DISCUSSION

Figure 1 clearly shows there is a fundamental difference in the transformation behaviours of the experimental N130B steel and the commercial P92 steel for peak temperatures near their respective A_3s. These diffraction data confirm that the transformation of the original tempered martensite structure to the equilibrium austenite phase is much more sluggish in N130B than in P92. This occurs even though the

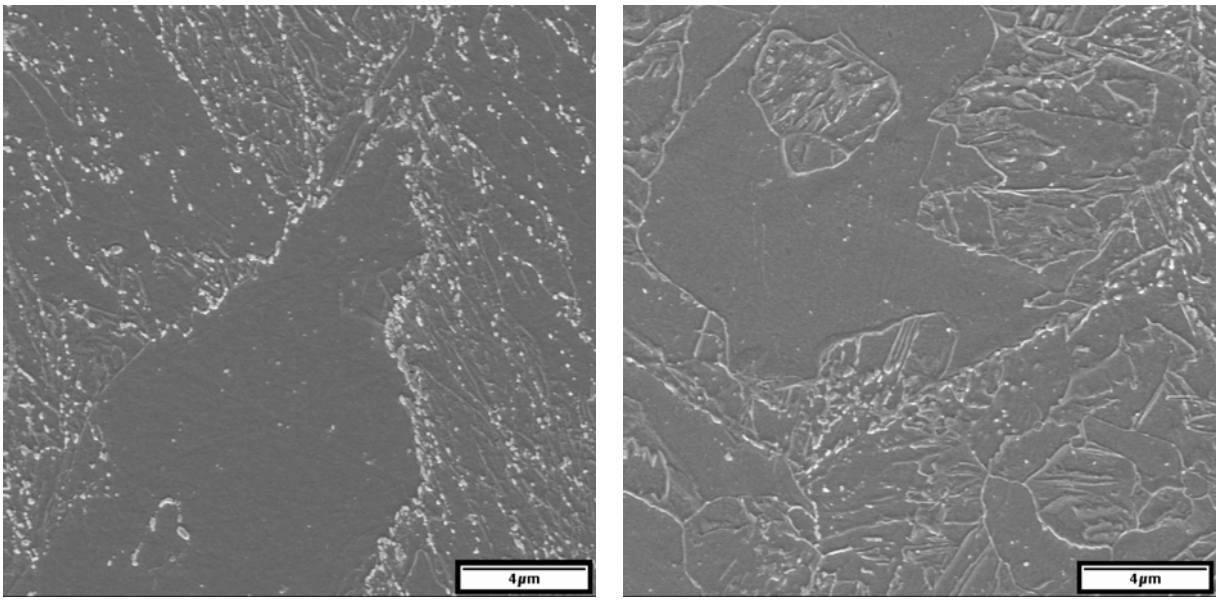

Figure 3 SEM micrographs showing the microstructures of (left) N130B and (right) P92 after heating through the respective thermal cycles shown in Figure 1

N130B is heated about 60°C above its calculated A_3 while the P92 is heated just to its A_3. Kobayashi et al [15] observed a similar effect using electrical resistivity measurements to follow transformations in two 9Cr steels of identical composition except that one contained 0.0098 wt% B. The starting condition of the steels was solution treated and quenched so that the progress of carbide precipitation during continuous heating (10°C/min) was also captured. Azuma et al [16] observed metallographically that 0.009 wt% B retarded the transformation of ferrite to austenite in 12Cr steels. They also observed that carbide dissolution was retarded in the B-containing alloy. The work of Kondo et al [10,11] indicates that austenite nucleation in a weld HAZ of the N130B steel is reduced compared to that in P92. The diffraction data are consistent with these studies relative to the effect of B on the transformation rate of ferrite to austenite.

The microstructures shown in Figure 2 and Figure 3 suggest that the carbide precipitates in N130B were much more stable than those of P92 for heating to temperatures near their A_3. The bulk of these visible particles are undoubtedly $M_{23}C_6$. Equilibrium thermodynamics calculations [14] indicate that both alloys will contain about the same total amount of $M_{23}C_6$, 1.7 vol% in N130B and 1.8 vol% in P92, and that the solution temperatures are 839°C in N130B and 858°C in P92. The compositions (at%) of the $M_{23}C_6$ particles in the N130B and P92 were also calculated at their respective tempering temperatures and they are given in Table 4. The $M_{23}C_6$ in both steels is predicted to contain similar levels of Fe, Cr, Mn, and V. One possibly significant difference is that $M_{23}C_6$ in N130B is expected to contain 3.9 at% B while that of P92 is much lower, 0.08 at%. Another difference is that $M_{23}C_6$ in P92 contains a much high amount of the refractory metal elements Mo and W compared to N130B. This information suggests that B may be more potent at stabilizing $M_{23}C_6$ against dissolution and coarsening than Mo and W.

Table 4 Calculated compositions of $M_{23}C_6$ carbides in N130B at 800°C and P92 at 780°C

	Composition, at%								
Alloy	Fe	Cr	Co	Mn	Mo	V	W	B	C
N130B	23.3	53.1	0.3	0.6	---	0.6	1.4	3.9	16.8
P92	21.6	50.8	---	0.8	3.5	0.6	2.1	0.08	20.6

The stability of the $M_{23}C_6$ carbides can also impact the ferrite-austenite transformation behaviour by removing C from solution. This would have the effect of artificially reducing the carbon concentration in N130B and increasing its A_3 relative to that expected based on bulk C concentration. The predicted sensitivity of A_3 to carbon concentration in a N130B base alloy is shown in Figure 4. Reducing the bulk/matrix C concentration clearly increases A_3.

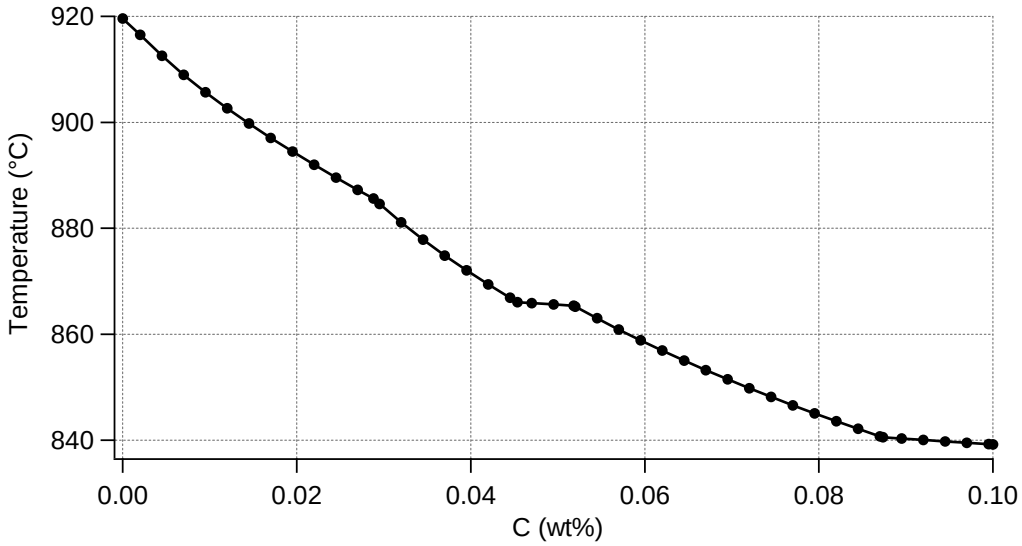

Figure 4 Calculated dependence of A_3 with C concentration in a base alloy of N130B composition

Taken all together, these data and analysis indicate that the stability against dissolution of $M_{23}C_6$ for short-time high-temperature exposures characteristic of fine-grained HAZs is increased in N130B by its elevated B concentration compared to P92. In addition, $M_{23}C_6$ that is more stable under these heating conditions would have the effect of increasing the apparent A_3 of N130B as the diffraction data confirm. An apparent increase of A_3 would make the ferrite-austenite transformation appear sluggish or difficult to complete for temperatures in the vicinity of the true A_3.

Whether the difference of transformation behaviour between N130B and P92 when heated through conditions characteristic of fine-grained HAZs is relevant to the resistance of high-B 9Cr steel to Type IV failure remains to be discovered. The hardness of the N130B microstructure in Figure 2, 2.57 GPa, is much lower that that of P92, 4.02 GPa. Based on this it might be expected that the regions of P92 weld HAZs characterized by peak temperatures in this vicinity would have better creep strength than those of N130B. Other detailed analysis of weld HAZ microstructures clearly indicates that the opposite is true [10,11,12]. The N130B structure shown in Figure 2 could certainly develop significant creep strength based on its still large fraction of small subgrains decorated with carbides. The possibility also exists of additional $M_{23}C_6$ precipitation from what was dissolved during the HAZ thermal cycle. Both of these could be sources of strengthening [4]. In contrast, P92 would have a much higher potential for $M_{23}C_6$ precipitation during subsequent tempering and creep testing because more of the initial distribution is dissolved. In addition, because P92 formed so much more new martensite as shown in Figure 1 it is likely to have a greater potential for dislocation hardening. The microstructures shown in Figure 2 and Figure 3 also suggest that the newly-formed prior austenite grain size of P92 is relatively small, even compared to the prior austenite grain size in its N+T condition. The prior austenite grain structure of N130B is much more non-uniform by comparison, and at least some of its original large austenite grain structure appears preserved.

Kondo et al [11] suggested that grain refinement in the fine-grained HAZ was avoided because B suppressed the nucleation of new austenite during heating. However, their work confirms that austenite nucleation was only suppressed at subgrain boundaries and not at the prior austenite boundaries. The thermodynamic calculations indicate that the equilibrium B concentration of ferrite in N130B at its 800°C tempering temperature is about 0.0001 wt%, and in P92 at its 780°C tempering temperature it is 0.00001 wt%. These B concentrations are well below those that are generally needed to influence nucleation of ferrite from austenite in carbon steels [17]. It is still feasible that the difference of prior austenite grain structure influences the suppression of Type IV failure in high B 9Cr steels like the N130B. However, it is also feasible that the thermodynamic and kinetic stability of carbides ultimately control their creep behaviour.

CONCLUSIONS

Synchrotron diffraction was used to follow the ferrite-austenite transformation in two 9Cr steels, an experimental 9Cr-3W-3Co-NbV steel with high B and low N (N130B) and the commercial alloy P92. Diffraction data were collected as the steels were heated through simulated weld heat-affected zone thermal cycles.

When heated to peak temperatures near 1100°C, both steels rapidly transformed from ferrite to 100% austenite. During cooling, both also transformed to martensite near 400°C. Both steels also retained untransformed austenite: 1.7% in N130B and 5.8% in P92.

Transformation behaviour near their respective A_3s was more complicated. When the N130B was heated to about 60°C above its A_3 of 847°C about 56% of the original ferrite never transformed to austenite. During cooling an additional 21% of ferrite and 23% of martensite formed. It retained no austenite. When the P92 was heated to just above its A_3 of 889°C. About 15% of the original ferrite never transformed to austenite. During its cooling an additional 22% of ferrite and 60% of martensite formed. This steel retained about 2.3% austenite.

Metallographic examinations indicated that the $M_{23}C_6$ in N130B was much more stable than that in P92 for heating to the lower peak temperatures. Analysis using equilibrium thermodynamics suggested that the more stable $M_{23}C_6$ in N130B could raise its apparent A_3 by sequestering C. Thermodynamic analysis also indicated that the $M_{23}C_6$ in N130B contained about 3.9 at% B compared to about 0.08 at% B in that of P92. In contrast, the Mo and W content of the $M_{23}C_6$ was predicted to be higher in P92.

ACKNOWLEDGEMENT

This research was sponsored by the Office of Fossil Energy, Advanced Research Materials Program, (DOE/FE AA 15 10 10 0) U.S. Department of Energy under Contract DE-AC05-00OR22725 with UT-Battelle, LLC. The APS is supported by the U.S. DOE, Basic Energy Sciences, Office of Science under contract No. W-31-109-Eng-38. Access to the SEM was through the SHaRE User Facility which is http://www.ornl.gov/bes/BES/microscopy/microsco.htm supported by the Division of Scientific User Facilities, Basic Energy Science Program, Office of Science, U.S. DOE. The technical assistance of S. S. Babu, J. W. Elmer, and T. A. Palmer were invaluable for conducting the experiments and analyzing the diffraction data.

REFERENCES

[1] H. K. D. H. Bhadeshia, "Design of Creep-resistant Steels," ISIJ International, 41 (2001), no. 6, pp.626-640

[2] J. M. Vitek and R.L. Klueh, "Precipitation Reactions during the Heat Treatment of Ferritic Steels," Metallurgical Transactions, 14A (1983), pp. 1047-1055

[3] W. B. Jones, C. R. Hills, and D. H. Polonis, "Microstructural Evolution of Modified 9Cr-1Mo Steel," Metallurgical Transaction, 22A (1991), pp. 1049-1058

[4] K. Maruyama, K. Sawada, and J. Koike, "Strengthening Mechanisms of Creep Resistant Tempered Martensitic Steel," ISIJ International, 41 (2001), pp. 641-653

[5] J. Hald, "Microstructure and Long-Term Creep Properties of 9-12% Cr Steels," pp. 20-30 in proceedings of 2005 ECCC Creep Conference

[6] C. R. Brinkman, V. K. Sikka, J. A. Horak, and M. L. Santella, "Long-Term Creep Rupture Behavior of Modified 9Cr-1Mo Steel Base and Weldment Behavior," ORNL/TM-10504, Oak Ridge National Laboratory, Oak Ridge, Tennessee, 1987

[7] F. V. Ellis and R. Viswanathan, "Review of Type IV Cracking," pp. 59-76 in PVP-Vol. 380, Fitness-for-Service Evaluations in Petroleum and Fossil Power Plants, ASME 1998

[8] J. A. Francis, W. Mazur, and H. K. D. H. Bhadeshia, "Type IV cracking in ferritic power plant steels," Materials Science and Technology, 22 (2006), pp. 1387-1395

[9] C. J. Middleton, J. M. Brear, R. Munson, and R. Viswanathan, "An Assessment of the Risk of Type IV Cracking in Welds to Header, Pipework, and Turbine Components Constructed from the Advanced Ferritic 9% and 12% Chromium Steels," pp. 69-78 in Proceedings of the 3rd Conference on Advances in Materials Technology for Fossil Power Plants, The Institute of Materials, London, 2001

[10] M. Kondo, M. Tabuchi, S. Tsukamoto, F. Yin, and F. Abe, "Suppression of Type IV Failure in High-B Low-N 9Cr-3W-3Co-NbV Steel Welded Joint," pp. 987-998 in Proceedings of the 4th Conference on Advances in Materials Technology for Fossil Power Plants

[11] M. Kondo, M. Tabuchi, S. Tsukamoto, F. Yin, and F. Abe, "Suppressing type IV failure via modification of heat affected zone microstructures using high boron content in 9Cr heat resistant steel welded joints," Science and Technology of Welding and Joining, 11 (2006), no. 2, pp. 216-223

[12] S. K. Albert, M. Kondo, M. Tabuchi, F. Yin, K. Sowada, and, F. Abe, "Improving the Creep Properties of 9Cr-3W-3Co-NbV Steels and their Weld Joints by the Addition of Boron," Metallurgical Transactions, 36A (2005), pp. 333-343

[13] J. W. Elmer, T. A. Palmer, S. S. Babu, and E. D. Specht, "In situ observations of lattice expansion and transformation rates of α and β phases in Ti-6Al-4V," Materials Science and Engineering A 391 (2005), pp. 104-113

[14] N. Saunders, "Fe-DATA, version 6, a database for thermodynamic calculations for Fe alloys," Thermotech Ltd., Surrey Technology Centre, The Surrey Research Park, Guilford, Surrey GU2 7YG, U.K.

[15] S. Kobayashi, K. Toshimori, K. Nakai, Y. Ohmori, H. Asahi, and T. Muraki, "Effects of Boron Addition on Tempering Processes in an Fe-9Cr-0.1C Alloy Martensite," ISIJ International, 42 (2002), Supplement, pp. S72-S76

[16] T. Azuma, D. Miki, and Y. Tanaka, "Effect of Boron on Microstructural Change during Creep Deformation in 12% Cr Heat Resistant Steel," pp. 177-186 in Proceedings of the 3rd Conference on Advances in Materials Technology for Fossil Power Plants, The Institute of Materials, London, 2001

[17] B. M. Kapadia, "Prediction of the Boron Hardenability Effect in Steel – A Comprehensive Review," pp. 448-480 in Hardenability Concepts with Applications to Steel, the Metallurgical Society of AIME, AIME, Warrendale, Pennsylvania, 1978